1'I,AN12'TAR% TOPOGRAPHY MAI' GENERATION

Meei nong Lee, Jean Lorre
Jet Propulsion Laboratory
California Institute of Technology
Pasadena Ca. 91109

Abstract

The planetary community is particularly challenged in pursuing digital elevation model generation due to: (I) limited multi-look observations and (2) the dynamic nature of the observation which introduces complex geometric relationships between observed body, spacecraft position, and sensor orientation. This paper presents two types of automatic planetary topography map generation tools developed at the Jet Propulsion laboratory [1]. The first tool extracts relative elevation from a true stereo pair based on a hierarchical image registration process employing a multi-resolution pyramid image representation method. The second tool analyzes the planet body shape from an arbitrary image pair with an overlapping area utilizing a common map projection space as a registration medium.

1 TN'1'JK)DUCYI'1ON

Surface topography is necessary for various scientific processing and analysis of planetary observation datasets including 2D image construction from the range information obtained by Radar systems, geometric correction of the off-nadir (oblique) angle observations, radiometric correction of the slope related shading, etc. The logic applied to distortion removal can be inversely applied to extract or upgrade digital elevation model (DEM). Multi-look stereo processing, photo/radar clinometry, and shape from shading are examples of such inverse processing techniques.

The inverse processing techniques are conceptually straight forward but they are mathematically as well as computationally very challenging to implement. The planetar y community has been additionally challenged due to the limited multi-look observations and the dynamic nature Of the observation which introduces complex geometric relationships between observed body, spacecraft position, and sensor orientation.

In the absence of a proper stereo database, the planetary community has resorted to photo/radar clinometry techniques [5] [3] [6] which utilize the intensity variation in a single look image to derive surface slope information. The clinometry techniques iteratively construct the surface slope model until the final solution is obtained which minimizes the intensity residual between the observation and the synthesized intensity based 011 apriori photometric/radiometric surface properties. The limited understanding of the photometric and radiometric properties of the planet surface and the computational complexities of the algorithms have been major drawbacks of the clinometry techniques.

During the recent Magellan SAR mission, cycle 111 of the mission was dedicated to observe the same area which was taken during cycle 1 with a different look-angle so that stereo processing can be applied for high resolution topography map generation of Venus. A multi-resolution stereo processing algorithm was developed to process large stereo datasets. The algorithm was implemented 011 parallel architectures employing data parallelism where the algorithm is parallely executed over a large number of nodes on decomposed datasets [7].

Another stereo algorithm was implemented which deals with an image pair with arbitrary scale and orientation. This method utilizes the navigation

information and planet body model to transform the images from sensor space (pixel location) to a 31) object space (latitude/longitude/radius) and to a 2D map projection space. The map projection space removes the Scale, rotation, and viewing geometry difference between the image pair so that the images can be registered for tiepoint generation. The tiepoints are reprojected onto the original image coordinate where the distance between a tiepoint pair is assumed to be introduced from either inaccurate planet body II model or surface elevation.

Both algorithms employ an areal correlation based 1 mage registration [1] process for determining the geometric disparities (tiepoints) between the two images. The major weakness of the areal correlation algorithm in terms of coping with either Very gradual or very abrupt elevation changes still persists in our implementations. An adaptive least square correlation [4] which takes into account the geometric distortion between the two different projection angles may improve some of the registration difficulties. Stereo processing followed by clinometry processing also provides an alternative solution to overcome the weakness.

2 HIERARCHICAL STEREO PROCESSING

2.1 Multi-resolution Representation

Multi-resolution pyramid representation developed by Burt et al. [2] consists of three operators, Reduce(R), Expand(E), and Laplace(L). The Reduce operator acts as a subsampler as well as a lowpass filter by applying a Gaussian filter on an image while decimating the image. The Expand operator enlarges the reduced image to the original size by reinserting the missing pixels with the lowpass filtered result of the neighboring area. The Laplace operator is a simple subtracter which acts as a highpass filter by subtracting the lowpass filtered image from the original image.

These operators are applied to an image successively to create image representation pyramids. The sequence of reduced images (low pass filtered images) is called Gaussian Pyramid and the sequence Of highpass filtered images is called Laplacian Pyramid. The Laplace operator acts as a bandpass filter when it is applied to an already lowpass filtered im-

age (Gaussian pyramid above level 0).

The relationship between three operators (R, E, L) is expressed as

$$G^{l+1} = R(G^l) \tag{1}$$
$$L^l = G^l - E(G^{l+1}) \tag{2}$$
$$G^l = L^l + E(G^{l+1}) \tag{3}$$

where the superscript l indicates the pyramid level.

One can utilize wavelet transforms to achieve a similar multi-resolution representation [8] [?]. The main objective in employing the multi-resolution representation is to extract the edges in a hierarchical fashion so that the image registration process can be more efficient as well as more robust.

2.2 Image Matching

The image matching process employs both Gaussian pyramid and Laplacian pyramids. The highest level of pyramids (level n) may be determined by building the pyramids until the correlation of the bandpass filtered images (Laplace pyramid level n) over an entire area is successful or it may be set to a reasonable level prior to the matching process. The Laplacian pyramid which extracts proper spatial frequency features for each level is applied for the correlation process. For noisy data, the correlation process must be avoided for the Laplacian pyramid level 0 since the high frequency features may be from noise. Figure 1 illustrates the pyramid level 3 image matching process and Figure 2 describes the relationship between the disparity, elevation, and prediction for the next level. The disparity is converted to elevation in each level prior to the expansion step and the expanded elevation is converted back to disparity in order to be used as a prediction for the next registration step. This step is necessary due to the symetricity assumption the expansion step employs. The extracted elevation from this process is relative elevation expressed in a sensor space. The sensor space mapping to the object space (planet coordinate) must be performed for final topography map generation.

For each resolution level, the template size is kept the same. The same size template in multiple resolution implies multiple size templates at a single

resolutio ion. For the areas with no Successful match, their predicted disparities are taken as possible disparities. Such substitution can be viewed as employment Of the larger template correlation result when the smaller template does not contain enough correlatable features. Thus, the resulting disparities reflect adaptive template size correlation where the template size is determined based 011 the area correlation result.

After correlation process is completed for each template over the entire search area, the correlation score array is examined for the maximum wi lue. The maximum correlation value is tested against the similarity threshold and the areas whose similarity is less than the threshold are either interpolated using neighboring disparity values (lowest resolution) or substituted with the predicted disparity. The true maximum location and score can be estimated by fitting a quadratic surface function shown below 011 the correlation score array.

$$S(x, \; y) = ax^2 + by^2 + cxy + dx \; \text{-1} \; cy \; \text{-1} \; j \quad (4)$$

$$dS/dx \; = \; 2ax + cy + d = 0 \quad (5)$$

$$dS/dy \; = \; 2by + cx + c = 0 \quad (6)$$

The polynomial function may be approximated without the xy term which allows an independent one dimensional quadratic function fit around the maximum correlation point. The values of a and b indicates the flatness of the surface. The surface flatness implies the ambiguity of the correlation. The correlation result may be ignored when the ambiguity is above a certain threshold.

3 MODEL BASED ELEVATION ANALYSIS

Stereo datasets are extremely rare for many planetary bodies. In order to extract elevation from an arbitrary (non-stereo) image pair, the second tool was developed. The philosophy is to acquire a massive set, Of tiepoints, one at every pixel, to solve for the intersection of the two view rays implied by each tiepoint pair, and then to interpolate a surface between the solutions to create images. The resulting maps are in absolute planetary coordinates with elevation in meters above the oblate spheroid. It is necessary to have accurate camera pointing matrices and the location Of each spacecraft in planet coordinates.

Figure 3 illustrates the algorithm structure. The algorithm takes an image pair in arbitrary orientation represented by Image1 and Image2. The raw images are then mapped to identical map projections using known navigation. It is unimportant what projection to use so long as they are the same. This step removes scale, rotation, and viewing geometry differences between the raw images. Note that these projections are locally in error due to parallax but we only use them for convenience and will later undo the projection for each tiepoint. The next step is 10 acquire a dense set of tiepoints which we call Tiepoint Generation in Figure 3.

A two dimensional correlation based image matching process discussed earlier is employed here as well. When the tiepoints have been acquired they are subject to an edit or which eliminates points which disagree with their neighbors in either of two ways:

- The vector lengths differ by more than a certain percentage.

- The vector pointing directions differ by more than asct angle.

The remaining points are then inverse projected from their locations in the projected map space to their locations in the imaging space. Each tiepoint pair is then converted into two View lays emanating from their respective spacecraft camera focal plane locations into space. The direction cosines of these rays are refered to as (a_1, b_1, c_1) and (a_2, b_2, c_2) arid their emanation points the spacecraft locations (x_1, y_1, z_1) and (x_2, y_2, z_2).

The spacecraft location comes from the orbit stale vector, and the direction cosines from the rotation matrix M which converts planet coordinates into camera coordinates.

$$\begin{pmatrix} a \\ b \\ c \end{pmatrix} = M \begin{pmatrix} x - x_c \\ y - y_c \\ -f \end{pmatrix} \quad (?)$$

where f is the camera focal length.

The planet surface location is the point in space where the two **View** rays come the closest together. A line which is perpendicular to both view rays contains the solution. This line intersects each **view** ray. To compute the first intersection point we must solve for the intersection of the three planes at (x, y, z).

$$a^* x + b^* y + C^* \% - (a^* x_1 + b^* y_1 - \{ c^* z_1)) = 0 \quad (8)$$

$$a_1^* x + b_1^* y + c_1^* z - (a_1^* x_1 + \{ b_1^* y_1 + c_1^* z_1)) = 0 \quad (9)$$

$$a_2^* x - 1\ b_2^* y - 1\ c_2^* z - (a_2^* x_2 - 1\ b_2^* y_2 - 1\ c_2^* z_2)) = O \quad (1\ O)$$

where

$$[a^*, b^*, c^*] = [a_1, b_1, c_1] X [a_2, b_2, c_2] \quad (11)$$

$$[a_1^*, b_1^*, c_1^*] = [a^*, b^*, c^*] X [a_1, b_1, c_1] \quad (12)$$

$$[a_2^*, b_2^*, c_2^*] = [a^*, b^*, c^*] X [a_2, b_2, c_2] \quad (13)$$

where X represents the cross product. The second intersection point cau be obtained in a similar manner. The solution is midway between the two intersection points and the miss distance of the view rays is the distance between them.

The last step is to convert the points into planet latitude, longitude, and radius, to subtract the oblate spheroid radius at that latitude, and to interpolate the elevation data. Results are remapped onto a projection for viewing.

4 RESULTS

Figure 4 shows an example stereo processing result applied to a stereo pair obtained from Magellan SAR on Venus. Figures 5 show an example of the model based elevation analysis applied to an image pair obtained from voyager II 011 a satelite of Uranus, Miranda.

The resulting elevation mode] shown in Figure 4.]) was verified by applying it to remove the geometric distortion introduced by the oblique look angle observation i from the raw images. The correction process is refered as au orthonormal projection which simulates an image taken from the nadir look angle. If the elevation model were accurately generated, the two orthonomal projection images would have identical spatial relationship. Though due to radiometric differences between two images

and noise added from resampling process, the difference is not entirely due to elevation model error, simple image differencing **may** be employed to **verify** the accuracy of the elevation. Figure 4.c illustrates the difference images before and after orthonormal projection which **clearly** indicates the elevation model **is** accurate in most areas.

References

[1] 1).1. Barnea, H. F. Silverman. *A class of Algorithms for Fast Digital Image Registration*, IEEE Transactions on Computers, c-21, N O . 2, 179-186, 1972

[2]]'. J. Bui 1. *Fast Filter Transforms for Image Processing*, Computer Graphics and Image Processing, pp 20-51, 1981

[3] I{.'J'. Frankot, R. Chellappa. *Application of a Shape from Shading Technique to Synthetic Aperture Radar Imagery*, Proceedings of IGARSS 1987 Symposium, A nn A rbor, pp 1,5'.?3-1,729, May 1987

[4] A.W. Gruen, E.P. Baltasavias. *Adaptive Least Squares Correlation with Geometric Contraints*, SPIE Vol. 595 Computer Vision for Robotics, 1985

[5] 11.1< .1' Horn, M. J. Brooks. *The variational Approach to shape from shading*, Computer Vision, Graphics, and Image Processing, Vol 33, pp. 1 7 . 4 - 2 0 8 , 1986

[6] R.L. Kirk. *A Fast Finite-Element Algorithm for Two Dimensional Photoclinom etry*, Ph. D. Thesis, California Institute of Technology, Pasadena, California, 1987

[7] S. Lewicki, M. Lee, P. Chodas, E. Dejong. *Stereo Processing of Magellan SA R Imagery Performed on a Transputer A rchitecture*, IGA RSS, Tokyo, Japan, 1992

[8] S. B. Mallat. *A Theory for Multiresolution Signal Decomposition, the Wavelet Representa - tion*, IEEE Trans. PA MI, vol. 11, pp 674- 693, 1989

Reference Image

Compared Image

GAUSS PYRAMID LAPLACE PYRAMID

LAPLACE PYRAMID GAUSS PYRAMID

LEVEL 0

LEVEL 0

Highpass

predicted
correlation

Highpass

1

bandpass 1

expand

ss 1

1

bandpass 1

2

predicted

2

bandpass 2

expand

bandpas ss 2

3

correlation

3
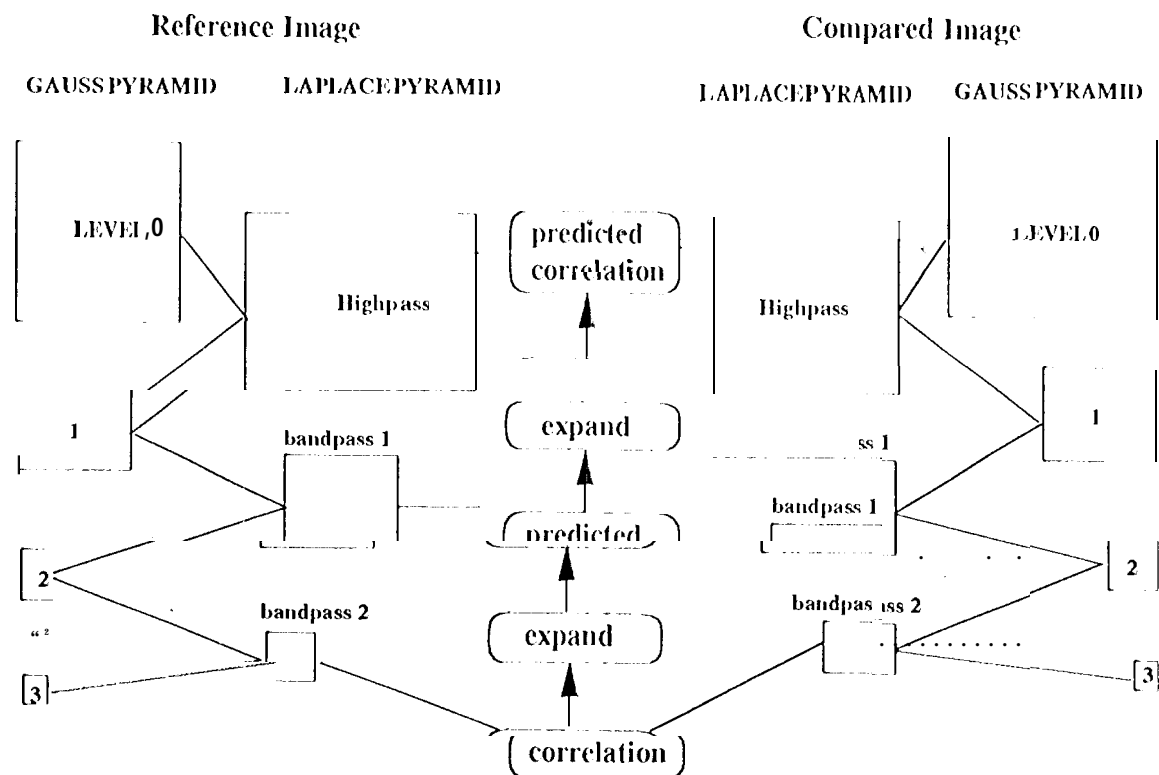
Figure 1. Multi-resolution Pyramid Stereo Processing

left image   right image

Multi–Resoluttion
Image Registration

Predicted
Disparity

Disparity to
Elevation

Expand

Elevation ro
Disparity

Sensor
Projection Model

Naviggation
Data

Topography
Map generation

Planelet
BodyModelel
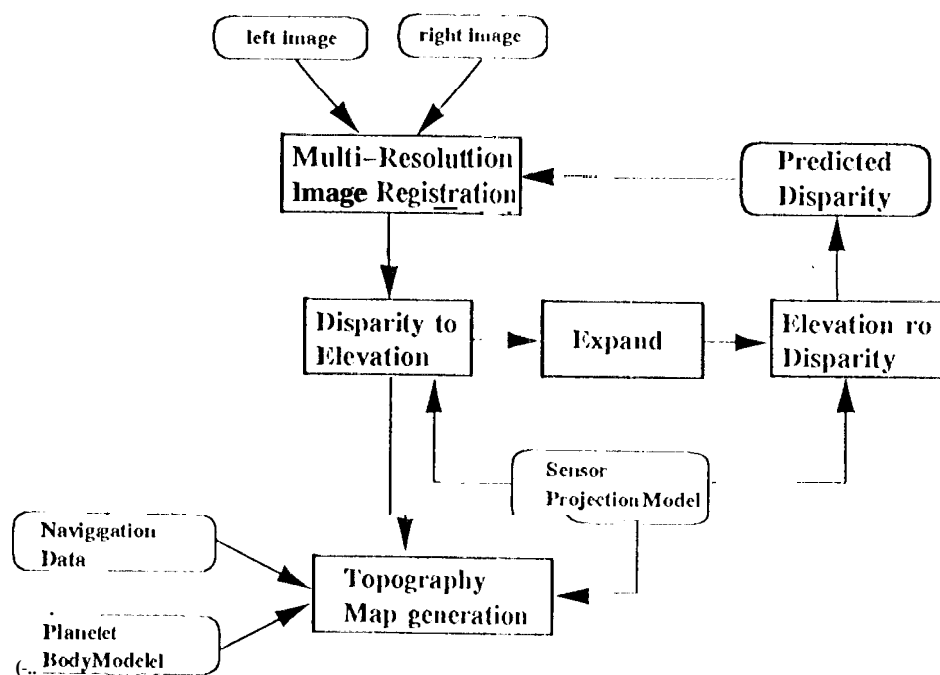
Figure 2. Elevation and Disparity
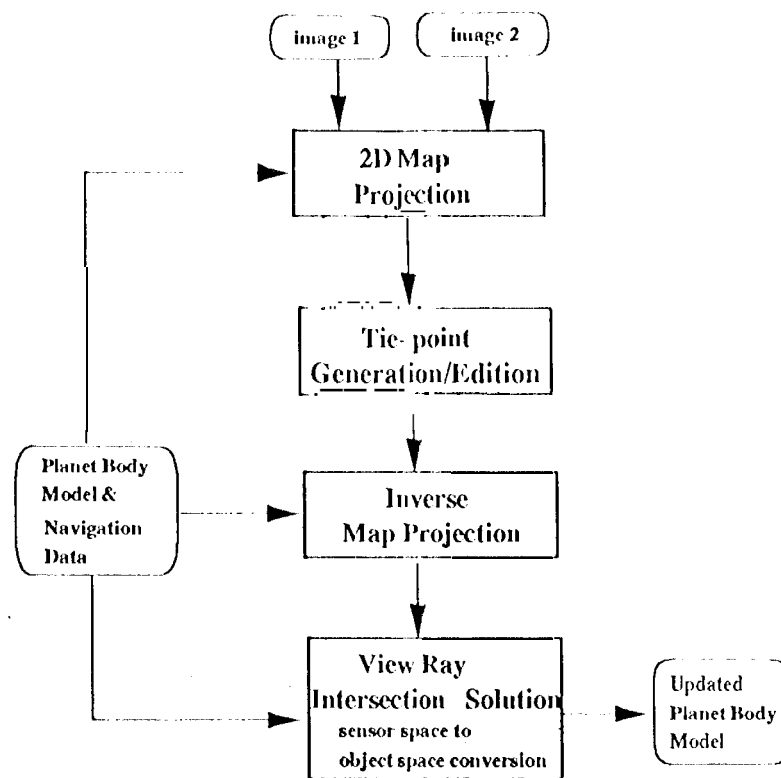
Figure 3. Model based Topography Map Generation Process
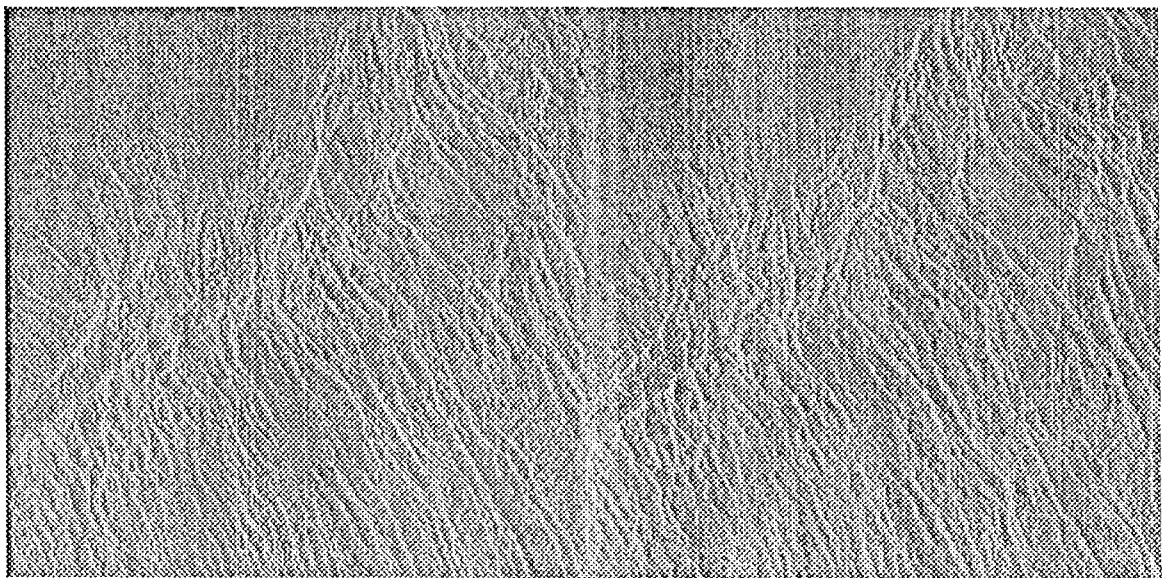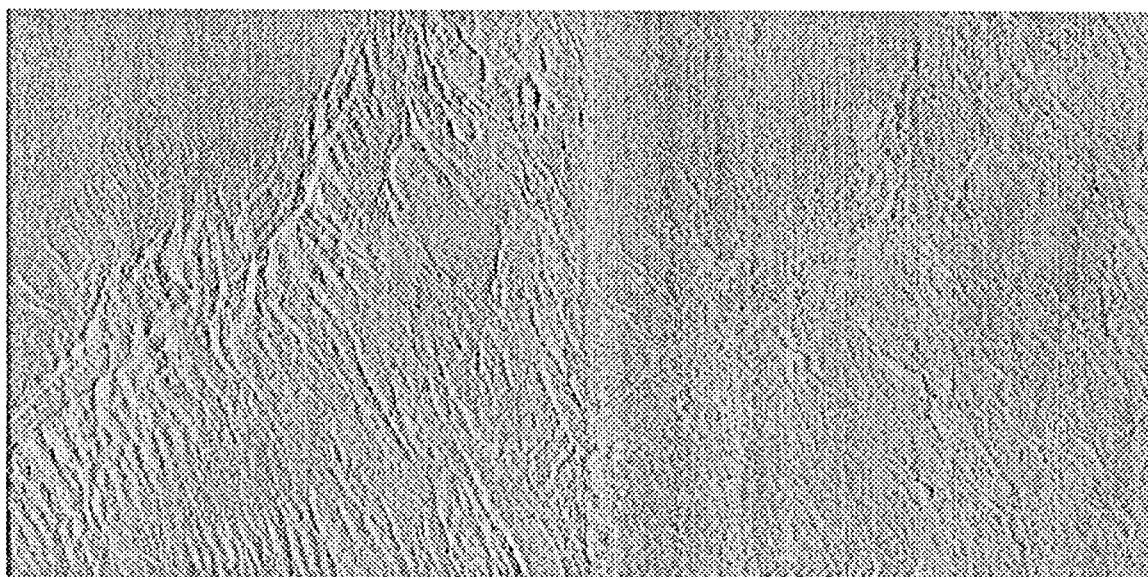

Figure! 4 .a
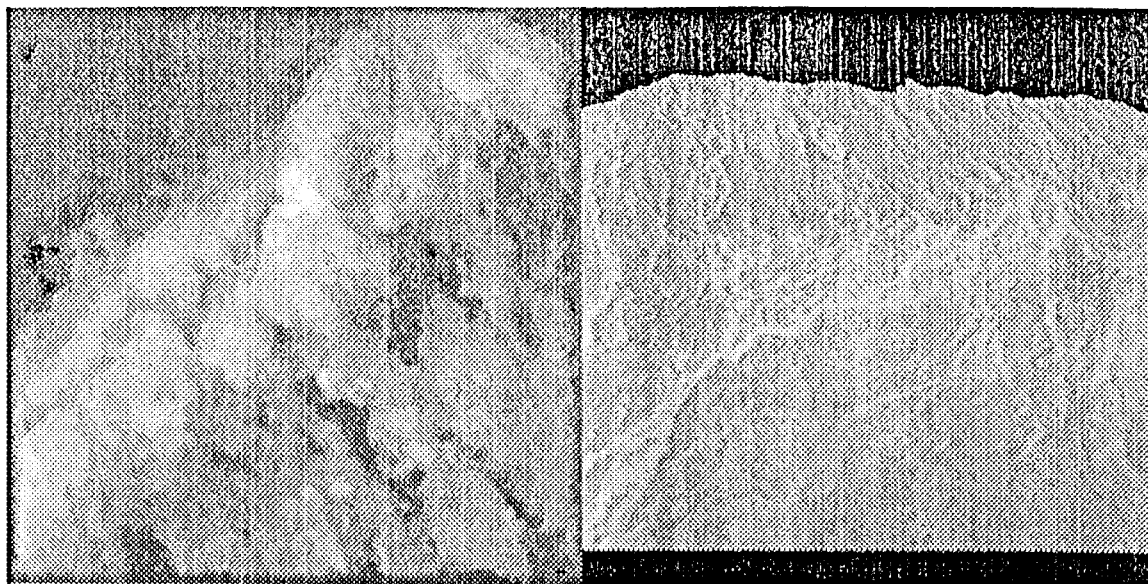
Figure 4.b

Figure 4.c

Figure 4 contains: a) a SAR stereo image pair of the Venus taken from the Magellan spacecraft, b) extracted elevation and a rendered scene, c) difference between the pair before and after orthonormal projection
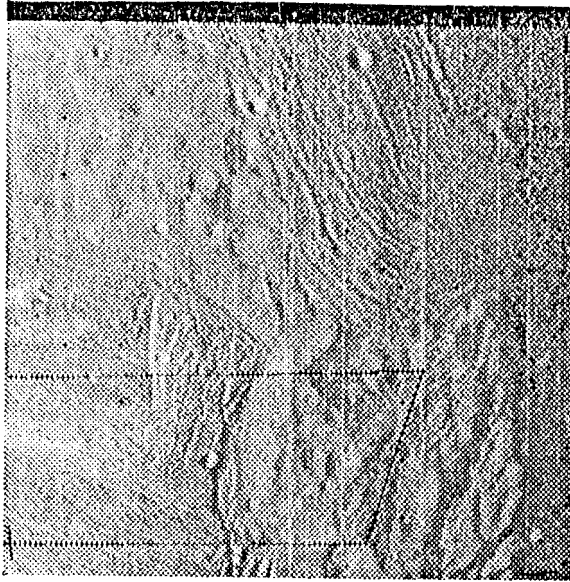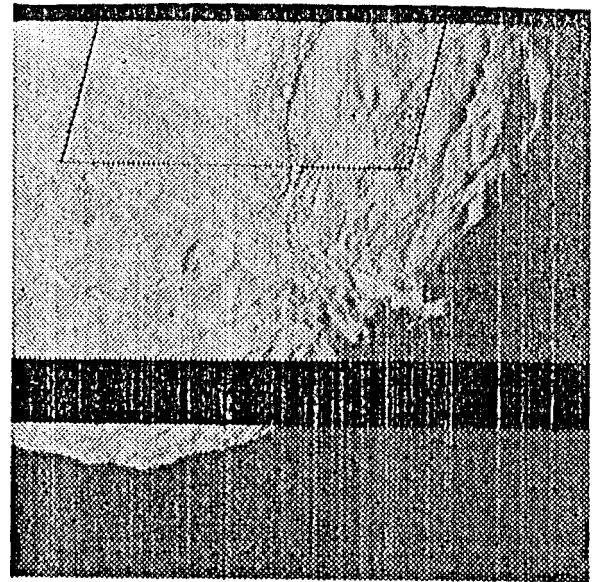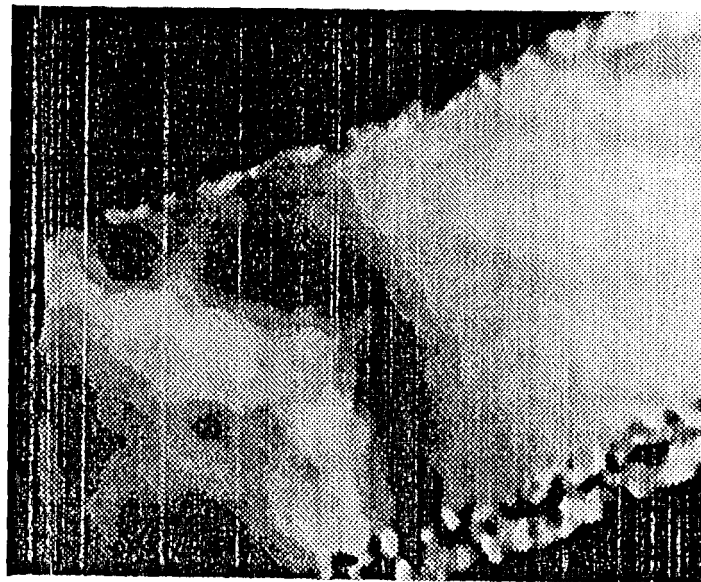
Figure 5.a

Figure 5.b

Figure 5.c

Figure 5 contains: a) Miranda image 2684617 (Uranus Encounter, Voyager II),
b) Miranda image 2684629 (Uranus Encounter, Voyager II),
c) Extracted Elevation in Map Projection Space